PCCP

Accepted Manuscript

ROYAL SOCIETY OF CHEMISTRY

www.rsc.org/pccp

Journal Name

Physical Chemistry Chemical Physics

Dynamic Article Links ►

ARTICLE TYPE

Modelling retinal chromophores photoisomerization: from minimal models in vacuo to ultimate bidimensional spectroscopy in Rhodopsins

Ivan Rivalta*[a,b], Artur Nenov[b] and Marco Garavelli*[a,b]

Retinal chromophores are the photoactive molecular units of visual and archaeal rhodopsins, an important class of light-activated biological photoreceptors. Extensive computational studies aimed to reveal the intrinsic photophysical and photochemical behavior of retinals in vacuo and the environmental effects that tune their properties in proteins and in solution are reviewed. Multiconfigurational and multireference

10 perturbative *ab initio* methods have been used to study retinal models with increasing size, from minimal to unreduced models. The hybrid quantum mechanics/molecular mechanics (QM/MM) approach has been employed for modeling retinals in solution and in proteins. QM/MM studies of the retinal photoisomerization in Rhodopsin, a prototype opsin protein responsible for peripheral vision, have provided fundamental understanding of the electrostatic effects regulating the spectral tuning in proteins

15 and have elucidated the photoisomerization mechanism with atomistic details, consistently with ultrafast optical spectroscopy experiments with sub-20-fs resolution. Different photochemical behaviors are observed for retinals in proteins and in solution. A molecular mechanism involving the interplay between ionic and covalent states during photoisomerization has been hypothesized but it remains uncertain and direct experimental evidences are lacking. Here, we propose transient bidimensional electronic

20 spectroscopy as a conceivable tool for obtaining key information on the retinal photoisomerization in different environments. Combination of computational techniques and ultimate ultrafast spectroscopy experiments could provide fundamental insights on retinals photochemistry and basic understanding for the design of biomimetic photochromic devices.

Introduction

25 Retinals are polyene chromophores responsible for light reception in opsins, the G protein-coupled receptors (GPCR) of the retinylidene protein family. Prokaryotic (type I) opsins harvest light energy to carry out metabolic processes, such as bacteriorhodopsin (bR) working as pump for proton transfers

30 across the cell membrane. In vertebrates, type II opsins are found in the photoreceptor cells (rod and cones) of the retina, where rod opsins (rhodopsins, Rh) are used for night and peripheral vision while cone opsins (photopsins) are highly sensitive pigments used for color vision. Rhodopsin is the only type II opsin for which the

35 X-ray structure has been resolved,[1-7] with a tertiary structure characterized by a bundle of seven transmembrane alpha helices (TM1-7, see Figure 1) linked by six loops (three in the cytoplasmic side, C1-3, and three in the extracellular side, E1-3). The chromophore in Rh is the 11-*cis*-retinal which covalently

40 binds the opsin apoprotein through a Schiff base linkage to a lysine residue in TM7, i.e. Lys296, forming an 11-*cis*-retinal protonated Schiff base (PSB11, Figure 1a). The absorption of visible light (with absorption maximum at ~500 nm) induces the 11-*cis*→all-*trans* isomerisation of the PSB11 (Figure 1b),

45 triggering protein conformational changes that start the signal transduction processes in the visual cascade.[8] The

photoisomerization of the retinal chromophore in Rh is the primary event in vision and a paradigm for fundamental studies of the molecular basis of vertebrate vision.

50 Beside the great biological relevance as visual opsin and, more generally, as prototype of the large GPCR family, visual Rh is the "natural" reference system for the design of bio-inspired photochromic devices.[9-11] In fact, retinals can be used as tunable chromophores that can be reversibly switched between different

55 absorption colors and, possibly, between light emitting and non-emitting states, with applications in biomimetic electronic devices and optical memories.[12] Fundamental understanding of the intrinsic photophysical and photochemical properties of retinal chromophores and environmental effects of the surroundings

60 (proteins, solvent, organic/inorganic supports, etc.) is crucial for the design of tailored photo-sensible devices.

Computational methods have been extensively used to sort out the intrinsic spectral properties and the photoisomerization reaction mechanism of retinal chromophores in vacuo.[13-31] In

65 particular, computational studies in our group have been focused, in the last fifteen years, on the photophysical and photochemical properties of retinal models of the protonated Schiff bases (PSB) present in Rh and bR, i.e. the 11-*cis* PSB11 and the all-*trans* PSBT, respectively, (Figure 1c).
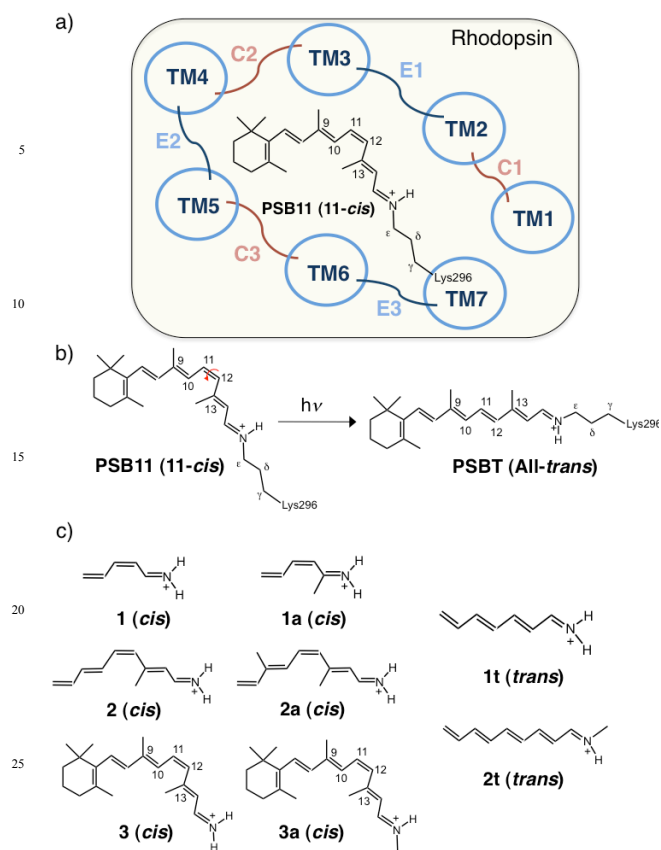
70

Figure 1. Schematic representation of the cis→trans photoisomerization reaction of PSB11 in Rhodopsin (panels a-b) and retinal chromophore models with different carbon chain lengths (panel c).

The computational approach used to obtain reliable spectral properties and excited state minimum energy paths (MEP) involves demanding *ab initio* methods, including geometry optimizations using multiconfigurational complete active space self-consistent field (CASSCF) theory[32, 33] followed by energy refinement at the second-order multi-reference perturbation theory (CASPT2) level,[34] to account for correlation effects (hereafter named CASPT2//CASSCF). The CASPT2 excitations are computed with the zero-order Hamiltonian shift (IPEA shift) sets to zero since the standard shift (0.25 eV) is proven to return worst results for the excited states of organic chromophores and polyenes, including retinal models.[30] While CASSCF excited state optimized structures of retinal models in gas-phase generally show a stronger bond inversion with respect to other levels of theory, such as coupled cluster, density functional theory, CASPT2, and quantum Monte Carlo,[30, 31] it has been shown that this difference is negligible in the protein environment, with CASPT2//CASSCF results showing good agreement with other methods.[31] So far, the CASPT2//CASSCF approach remains the only methodology that provides coherent photophysical and photochemical data for retinals in different environments, including vacuo,[23] solution[35] and protein,[35] consistently with absorption spectroscopy,[23] Resonance Raman,[20] chiroptical data,[36] and ultrafast optical spectroscopy experiments.[37]

Following the improvement of both algorithms efficiency and computer performances in the last two decades, we have firstly investigated minimal size retinal models and then larger models up to complete atomistic models of the PSBs. For instance, CASPT2/CASSCF studies of the minimal model of PSB11, with only three C=C bonds (model **1**, Figure 1c), and successive investigations of larger PSB11 and PSBT models with longer polyene chains and with methyl groups substituents (models **1a**, **2-3**, **2-3a**, **1t** and **2t**, Figure 1c) have provided fundamental insights into the intrinsic photoisomerization process of retinal chromophores, suggesting a *barrierless* relaxation of the spectroscopic state (S_1) that ends at a twisted conical intersection (CI) point, providing a fast and efficient route to the photoproduct. The reaction coordinate on the S_1 surface is characterized by two distinct reactive modes, first skeletal deformations then torsions about the reacting double bond. CASPT2/CASSCF calculations of isolated chromophores in vacuo have also shown that the ionic S_1 state and the covalent S_2 state do not interact along the isomerisation path. This photoisomerization mechanism, known as the *two-state two-mode* (TSTM) model,[21] has been also observed for unreduced PSB models, consistently with time-resolved spectroscopy experiments in various (protein and solution) environments.[38-43]

The inherent photochemical properties of isolated retinal chromophores in vacuo could not provide straightforward explanation for the differences in spectral properties, photoreaction rate, efficiency and selectivity experimentally observed for retinals in protein and in solution. In fact, the absorption maximum of retinals in opsins (e.g. 500 and 568 nm in Rh and bR, respectively) is significantly red-shifted with respect to the values of solvated chromophores (~440 nm), a phenomenon known as *opsin shift*. Moreover, while the photoreactions in Rh and bR lead uniquely to the photoproducts in ~200 and ~500 fs, respectively, with a quantum efficiency (QY) >60%,[44-47] retinal chromophores in solution (methanol or hexane) show much longer excited-state decay time (2-3 ps), poorly selective photoreactions and low QY (~25%).[48-51] Several factors can alter the intrinsic properties of retinal chromophores when they are embedded in proteins or dissolved in solution, including structural effects, such as equilibrium geometries and steric interactions, and electrostatic interactions, such as counterion effects and charge quenching. *Ab initio* methods have been used to elucidate specific electrostatic effects on the photophysical properties and photochemistry of PSB chromophores.[52, 53] For instance, correlation between the counterion position relative to the PSB polyene chain and the energy gaps between the S_0 (ground state, GS), S_1, and S_2 excited states has been observed (*counterion effect*). A simple electrostatic model can provide rationalization of the level energies calculated for isolated (i.e. in vacuo) tight ion pairs. When the (negatively charged) counterion is close to the N-end of the PSB, the covalent (S_0 and S_2) states are stabilized with respect to the ionic S_1 state due to the different charge distributions of these states. While the counterion effect can alter significantly the spectral properties and the photochemistry of retinals, the environment can quench/shield such electrostatic effect (*counterion quenching*). The hybrid quantum mechanics/molecular mechanics (QM/MM) approach has been used to evaluate such counterion quenching effect in different environments (proteins and solution).[35, 54, 55] By accounting for electrostatic embedding at the (multireference) QM level,

accurate electrostatic effects of the surroundings have been determined for the PSB11/counterion bound ion pairs in Rh and methanol solution.[35, 54] While in the Rh binding pocket a significant counterion quenching effect (almost half the whole counterion effect) is observed, bound ion pairs in solution and in vacuo have almost negligible quenching effect. Thus, electrostatics play a major role in regulating photophysical and photochemical properties of retinals.

In this work, we review our computational studies of retinal chromophores photoisomerization, starting from the earliest minimal model of PSB11 in vacuo[17] to the most recent QM/MM modeling of Rh which has shown quantitative agreement with ultrafast optical spectroscopy experiments.[37] Synergistic computational and experimental studies have provided fundamental insights on the retinals photochemistry, elucidating the intrinsic behavior of these chromophores and the important role of environmental effects, and presenting the molecular movie of the photoisomerization process in Rh with atomistic details and femtosecond resolution. However, the reasons behind the different behavior of retinals in protein and in solution remain uncertain. Computational studies and the experimental data available point to a different interplay between the covalent (S_0 and S_2) states and the ionic (S_1) state as function of the environmental conditions, with the covalent S_2 excited state being involved in the photoisomerization of solvated retinals (following a *three-state* model) and not in the proteins (*two-state* model). However, direct evidence of these two distinct mechanisms is not straightforwardly achievable with standard time-resolved (one-dimensional, 1D) pump-probe or femtosecond-stimulated Raman spectroscopies. Here, we propose transient bidimensional (2D) optical spectroscopy with elaborate multi-pulse sequences as the ultimate experiment to provide fundamental information on the relative positions of the singly excited states (S_1 and S_2) along the photoisomerization path of retinals in different environments. In fact, combination of transient 2D spectroscopy and accurate theoretical simulations of 2D electronic spectra could deliver decisive information on retinals photochemistry.

Retinal models in vacuo

The minimal retinal model

The *tZt*-penta-3,5-dieniminium cation (*cis*-$C_5H_6NH_2^+$, model **1**), a simple triene PSB cation, has been taken as minimal model of PSB11 since, despite its small size, it features a polyene ($H_2C=CH-$) and a polyeniminium ($-CH=NH_2^+$) moieties separated by a "central" *cis* double bond, in analogy to the 11-*cis*-retinal chromophore where the central 11-*cis* double bond is comprised between a butadienyl (ionone-HC=CH-CH=CH-) and a propeniminium (-CH=CH-CH=NH_2^+) conjugating residues. The MEP for photoisomerization of **1** has been investigated using CASSCF and CASPT2.[17, 18]

Figure 2 shows the photoisomerization path of **1** upon excitation to the spectroscopic ionic (${}^1B_u$-like) S_1 state. The calculated MEP of **1** indicates a *barrierless* relaxation of S_1 that ends at a CI point, where the S_1 and the S_0 surfaces cross. The CI is characterized by a ~80° twisted central double bond, providing a route for a fast and efficient nonadiabatic *cis→trans* isomerization. Notably, the S_2 covalent (${}^2A_g$-like) state lies at

high energies along the MEP, suggesting that it is not involved in the photoisomerization reaction (Figure 2a). Characterization of the changes in the molecular structure and charge distribution along the MEP of **1** revealed crucial aspects of the photoisomerization path in retinal chromophores. The initial acceleration determined by the excited state (S_1) energy gradient at the Franck-Condon (FC) structure induces a relaxation along a mode which involves the stretching of the C=N and the terminal C=C bonds and subsequent stretching of the central double bond, eventually resulting in a large lengthening of all formal double bonds and shortening of all formal single bonds. Deformation along this totally symmetric stretching mode occurs on topologically stable valley which morphology changes to a ridge when the torsional motion is initiated, originating a bifurcation point (BP). Along the MEP, the BP point is avoided with the twisting motion dominating the reaction pathway, giving rise to the actual *cis→trans* isomerisation (Figure 2b). Charge redistribution along the MEP indicates that the positive charge initially located at the $-NH_2$ molecular end smoothly migrates localizing on the CH_2CHCH- moiety, with the S_1 and S_0 charge distributions at CI showing a net one-electron transfer between the CH_2CHCH- and $-CHCHNH_2$ rotated moieties (Figure 2c), giving rise to a twisted intramolecular charge transfer (TICT) state. The charge redistribution continues along the MEP after the CI (i.e. on the GS branch), with the positive charge shifting back to the $-NH_2$ molecular end, as expected for the *trans*-$C_5H_6NH_2^+$ photoproduct.
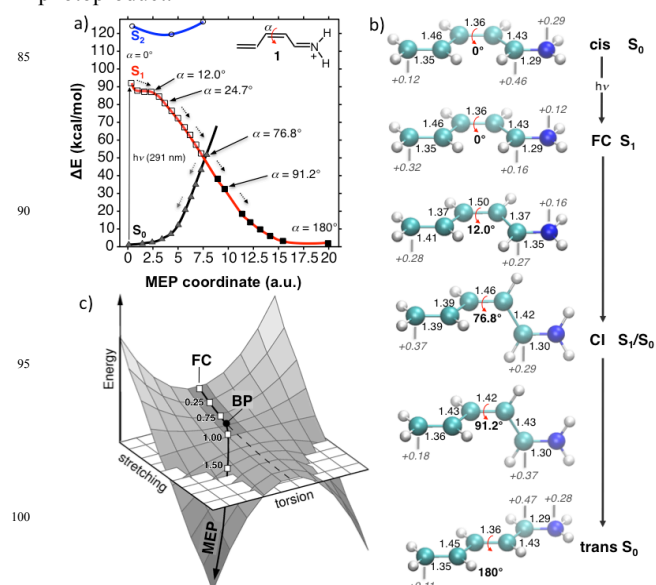

Figure 2. *Cis→trans* photoisomerization of the minimal retinal model **1** in vacuo. Panel a: energy profiles of the ground state (S_0, black line) and excited states (S_1 and S_2, red and blue lines, respectively) along the MEP describing the S_1 relaxation from the FC to the CI (open squares) and from the CI to the all-trans photoproduct (full squares) or back to the GS cis reactant (gray full triangles). Open circles show the S_2 state energies along the excited state branch of the photoisomerization path. Panel b: geometrical parameters (bond distances in Å and central torsion angle, i.e. α, in degrees) and selected atomic partial charges showing the structural and charge distribution changes along the photoisomerization path. Panel c: schematic representation of the energy landscape at the early stage of the photoisomerization path, showing the *two-mode* components of the MEP and the energy ridge where the bifurcation point (BP) is located. Reproduced from Ref. [17]

The computed MEP of **1** and the characterization of the CI point suggest a picture of the photoisomerization process that is consistent with a barrierless and fast excited state decay, in nice agreement with the short time scale (sub-picosecond) determined for the photoinduced PSB11 isomerization in proteins. Thus, the minimal model **1** already provides a suitable *ab initio* model for rationalizing the fast isomerization dynamics of the rhodopsin retinal chromophore. Considering the ionic character of the spectroscopic S_1 state and the charge distribution changes observed along the MEP, electrostatics are expected to play a crucial role on the rate and quantum yield of the retinal photoisomerization processes.
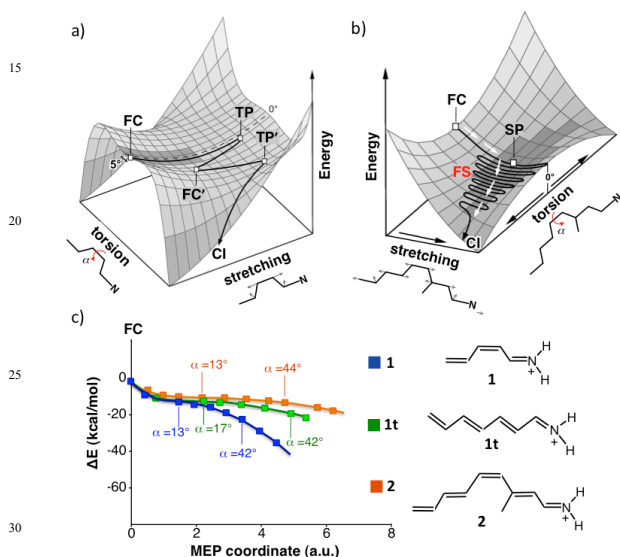

Figure 3. Comparison of the photoisomerization paths of retinal models with different carbon chain lengths (models **1**, **1t** and **2**) in vacuo. Panel a: schematic representation of the S_1 energy surface of **1**, with full line representing the calculated semiclassical trajectory. Panel b: the S_1 energy surface of **2,** with arrows indicating the relaxation path and full line represents a hypothetical classical trajectory released near FC with a small initial torsional perturbation. SP indicates the fully relaxed planar stationary point (energy minimum) and the shaded area corresponds to the transient fluorescent state (FS). Panel c: comparison of CASPT2-scaled MEPs computed for chromophore models with different chain lengths (**1**, **1t** and **2**). The twisting angles (in degrees) along the paths are also reported. Reproduced from Ref. [18, 19, 68]

Computations of the MEP provide a static picture of the photoisomerization process that could be very useful to elucidate fundamental aspects of the involved photochemistry, but they lack of direct information on the reaction dynamics, limiting to a qualitative comparison with experimental data obtained with time-resolved spectroscopy techniques. In an effort to obtain direct information on the photoisomerization dynamics of model **1**, *ab initio* on-the-fly semiclassical dynamics using CASSCF gradients[33] and surface hopping method[56, 57] have been performed.[18] Figure 3a shows the potential energy surfaces of the spectroscopic state of model **1** in the space of the skeletal deformations (the stretching modes involved in the initial part of MEP) as well as the torsion along the central double bond (α). A series of molecular dynamics simulations have been performed from the reference S_1 state (at the planar FC structure) and from more realistic slightly twisted configurations (at different small α values) to include intramolecular vibrational energy redistribution

(IVR) into the torsional mode, indicating that the CI point can be reached only by redistribution of the energy to nontotally symmetric (torsional) coordinates.

As shown in Figure 3a, starting with an initial twist of 5° the excited molecule moves along a trajectory that parallels the static MEP (dashed line in Figure 3a) within the symmetric valley determined by the skeletal deformations and orthogonal to the torsional mode. In contrast to the MEP, the trajectory shows one oscillation along the valley (from FC to FC') before the twisting motion begins, sampling large central bond distances. Where the curvature of the surface along torsional mode becomes negative (TP and TP' points) the system gains momentum along the *cis→trans* isomerization coordinate, with relaxation toward the S_1/S_0 crossing region starting after ~50 fs after the vertical excitation, the CI point being reached at 60 fs and the photoproduct being formed at 90 fs. These results have been later corroborated by ensemble calculations (studying up to 2000 trajectories) at various levels of theory.[26, 58] Large skeletal oscillations within 50 fs and the IVR to a torsional mode before acceleration toward the *cis→trans* isomerisation motion are consistent with the transient "fluorescent state" (FS) experimentally observed for several protein PSBs and PSBs in solution,[44, 48-50, 59-63] in agreement with the mechanism suggested by the pioneering semiempirical simulations carried out by Warshel and co-workers [64-67] and in line with subsequent computational studies on larger retinal models.

Methylated and long carbon-chain models

The minimal retinal model **1** contains only three out of the six double C-C bonds of PSB11 and does not include the methyl groups substituents. CASPT2/CASSCF studies of the photoisomerization process suggested that the inclusion of one methyl group in model **1** (model **1a**) modifies the MEP, with a 2-fold increase in the slope of the initial part of the S_1 isomerization path, in agreement with the increased reaction rate observed experimentally.[17] Several computational studies have been subsequently performed on the 4-*cis*-γ-methylnona-2,4,6,8 tetraeniminium cation (model **2**) and the its γ,η-dimethyl analogue (model **2a**), PSB11 models with five C-C double bonds. Figure 3b shows the comparison between the CASPT2/CASSCF energy profiles calculated for the S_1 states of the PSB11 models **1** and **2**, and the all-*trans*-hepta-2,4 ,6-trieniminium cation (model **1t**), a PSBT model with four C-C double bonds. The calculated MEPs for retinal models with four and five double bonds confirm that the initial acceleration out of the FC region is controlled by skeletal deformation, in analogy to what was observed for the minimal model. On the other hand, in the region dominated by the torsional deformation about the central double bond the energy profile is significantly affected by the length of the carbon chain, with longer chains showing an energy plateau that is absent in the minimal model (Figure 3).[19, 20, 68] In long carbon-chain models the flat planar stationary point (SP) is reached right after initial stretching relaxation, with the molecule ending up in a region of the S_1 energy surface where increasing the *cis→trans* isomerisation angle up to 40° leads only to a very small change in energy. Thus, the chromophore could perform several skeletal oscillations while sampling different torsional angles in this flat region and until vibrational energy redistribution from stretching (totally symmetric) modes to torsional modes drives the system to

the CI region (Figure 3b). The agreement between computed photophysical properties of model **2** and available experimental data of PSBs in solution and in proteins, including absorption and fluorescence maxima, changes in the S_1-S_0 dipole moments,[21] and resonance Raman spectra,[20] provides a validation of the quality of the model and the computational protocol employed. The reaction mechanism determined for model **2** is consistent with the "fluorescent state" (FS) observed in PSB11. However, the FS has different lifetimes in solution (~3ps in methanol)[48] and in rhodopsin (50-150 fs),[44, 69, 70] suggesting that other (non intrinsic) factors can shape the energy profile of the ionic S_1 state, including the interplay with covalent states of PSB11.

The two-state two-mode model

Two photophysical models have been proposed by experimental and computational studies[47, 71, 72] for the photoisomerization path of the PSBT in bacteriorhodopsin: a *three-state* [71, 72] and a *two-state* model[47] (Figure 4a-b). In the three-state model, an avoided crossing between S_1 and the second excited state (S_2) is predicted along the reaction path, giving rise to a transition state (TS) and a small barrier on the S_1 energy profile (Figure 4a). Instead, in the *two-state* model the S_1 relaxation is a barrierless process leading from the FC directly to the CI (Figure 4b). In both these two mechanisms the reaction coordinate is supposed to be *single-mode*, with the torsion about the reacting double bond driving decay along the S_1 energy surface.
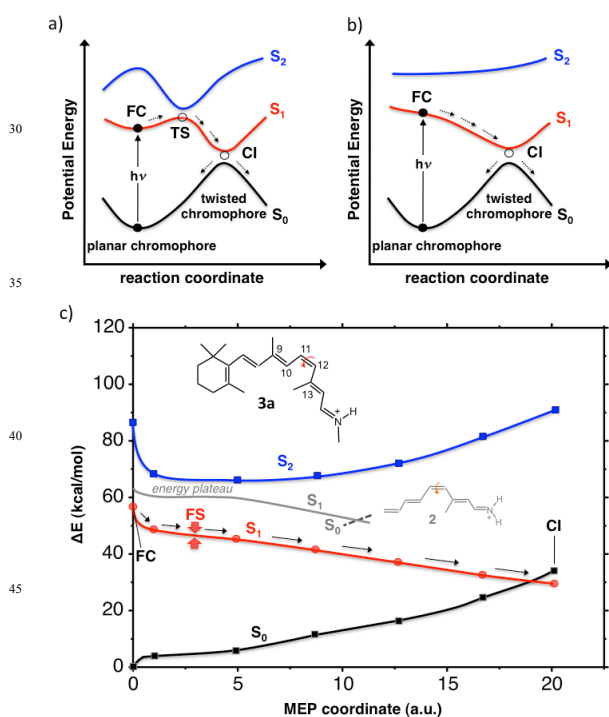

Figure 4. The *three-state* (panel a) and the *two-state* (panle b) photoisomerization mechanisms of retinals, with avoided crossing between the S_1 (in red) and the S_2 (in blue) surfaces giving rise to a transition state (TS). Panel c: comparison of the MEPs of model **2** and model **3a** calculated at the CASPT2 level of theory, with gray lines showing the MEP of model **2**. The fluorescent state (FS) in model **3a** is assigned at 3 a.u. (red arrows). Reproduced from Ref. [20, 68]

The two-state single-mode model has been also proposed for the photoisomerization of the PSB11 in rhodopsin proteins.[46, 73, 74] As shown in the previous sections, the intrinsic photochemical

behavior of PSB11 and PSBT retinal models involves a *two-mode* (first stretching then torsion) photoisomerization path. These results have been corroborated by computational analysis of the photoisomerization path of the *real* (i.e. unreduced) PSB11 in vacuo,[68] i.e. models **3** and **3a**. Figure 4c shows the MEP of the unreduced PSB11 model in vacuo (model **3a**), indicating that the S_1 and S_2 states do not interact via an avoided crossing and that a FS is predicted on the S_1 surface, in analogy to model **2**. The reaction path on the S_1 energy surface is characterized by a barrierless twisting about the central double bond, according to the *two-state* scheme (Figure 4b).

Therefore, the CASPT2/CASSCF studies of isolated retinal models suggest a *two-state two-mode* (TSTM) model for the photoisomerization of retinal chromophores in vacuo.[21] This mechanism has been also proposed by time-resolved spectroscopy experiments on retinal proteins (i.e., Rh and bR) and retinal chromophores in solution.[38-43]

The MEP calculated for the unreduced model **3a** (Figure 4c) suggests that the inclusion of the β-ionone ring in the retinal model affects only partially the photoisomerization mechanism (model **3a** versus model **2** in Figure 4c), with a steeper energy profile in the FS region observed in presence of the β-ionone ring.[68] Moving from the FC to the CI region a planarization of the ring is observed in vacuo, suggesting that steric interactions between the β-ionone and the protein environment would force an early twist of the central double bond and speed-up the photoisomerization in rhodopsin.[68] In the following section we analyze other factors that could affect the topology of the spectroscopic state energy surface and the interplay between ionic and covalent states along the photoisomerization path.

Environmental electrostatic control

Environmental effects play an important role in different aspects of the retinal photoisomerization, including reaction rates, selectivity, quantum yields (QYs) and efficiency. For instance, the excited-state of PSB11 in Rh decays monoexponentially with a lifetime of ~150 fs, leading to the unique all-trans PSBT photoproduct in ~200 fs and with a 67% QY.[44-46] Analogously, the PSBT in bR has a 200 fs lifetime, a reaction rate of ~500 fs and 65% QY for the 13-cis PSB13 photoproduct.[45, 47] In contrast, retinal chromophores in methanol (or hexane) solution feature a biexponential decay of the excited-state with a dominant shorter component of 2-3 ps, a low 25% QY and poor selectivity, with formation of a mixture of different stereoisomers.[48-51] Computational studies have been performed to disentangle solvent effects that affect photophysics and photochemistry of PSBs, including steric hindrance of the torsional motions,[75] proton transfer,[76] and electrostatic effects.[77] A spectral tuning, also known as *opsin shift*, is also observed as a function of the environment, with the absorption maximum in proteins (500 and 568 nm in Rh and bR, respectively) being red-shifted with respect to the chromophores in solution (around 440 nm). In this section we review computational studies of retinal models in vacuo and in protein that have elucidated fundamental aspects of such environmental control, where electrostatic interactions between the cationic PSB chromophore and the surrounding charges (e.g., its counterion) may play a major role.

The counterion effect

One dominant factor that modulates the environment dependent photophysics and photochemistry of PSBs, is the direct interaction between the positively charged PSB chromophore and its counterion. *Ab initio* multireference methods have been used to provide a unified view of the specific countercharge intermolecular effect on the photophysical properties and photochemistry of retinal chromophores.[52, 53] The countercharge effect has been assessed by computing the photoisomerization MEPs and the relative stabilities of the S_0, S_1, and S_2 states for the retinal models in vacuo (models **1-3**, including the five double bond PSBT model **2t**) as a function of the counterion positions (Figure 5).
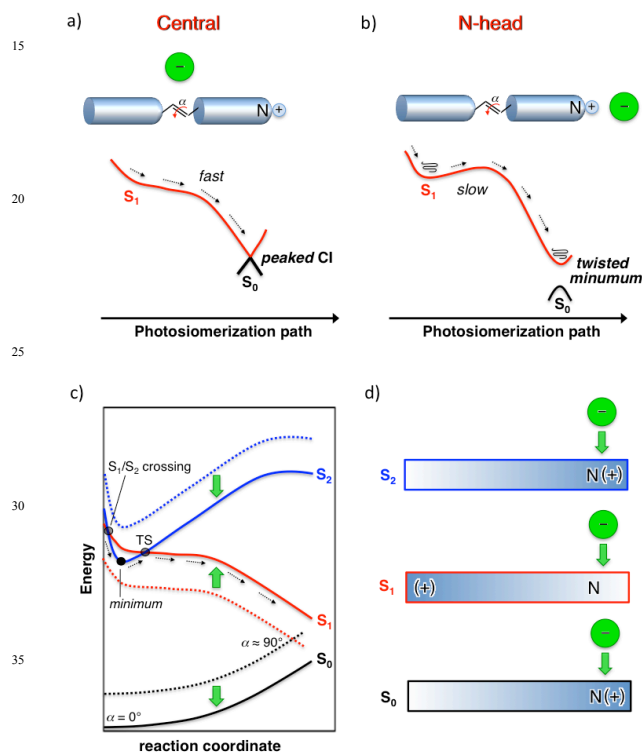

Figure 5. The counterion effect on the photoisomerization path of retinal models in vacuo. Panel a,b: schematic representation of the effect of the counterion position on the energy profile of S_1. Panel c: the counterion effect on the energy profiles of S_0, S_1 and S_2 states (full lines) in a tight ion pair with respect to isolated chromophore (dotted lines). Panel d: the positive charge distribution in the S_0, S_1 and S_2 states of tight ion pair , with horizontal smoothed colored bars representing the PSB skeleton. Reproduced from Ref. [52]

A comprehensive analysis of several MEPs involving *cis→trans* isomerisation about different C-C bonds suggest that the relative position of the counterion with respect to the carbon chain can shape the energy profile of the spectroscopic state along the photochemical path. As shown in Figure 5a, when the counterion is placed nearby the central ("twisting") double bond the S_1 energy profile resembles that of the isolated chromophore, with a steep and barrierless reaction path leading to a peaked CI. In this scenario a fast and efficient photoisomerization process is expected. On the contrary, if the counterion is located in the proximity of the N-head of the retinal chromophore, in analogy to retinal PSB chromophores in solvents (where such ion pairs are expected) and to Rh (with PSB11 and its counterion amino acid

residue Glu113 (E113)), the S_1 surface is significantly altered with respect to the isolated chromophore case, featuring a much flatter profile in the initial part, with a possible energy barrier and a twisted minimum at the bottom of the MEP. The energy barrier and the twisted minimum would delay the radiationless decay process, suggesting that the presence of a tight ion pair would decrease the rate, efficiency and selectivity of the photoreaction.

A simple electrostatic model can explain the counterion modulation of the retinal models photochemistry in vacuo (Figure 5c). In fact, the photochemically relevant S_1 state is a "hole-pair" charge transfer state with a positive charge localized at the C-tail of the retinal molecule, while the S_0 ground state and the "dot-dot" S_2 state are covalent states with the charge localized at the N-head of the PSB. For simple electrostatic reasons, a negatively charged counterion placed at the N-head stabilizes the covalent states and destabilizes the ionic state relatively to S_0 and S_2.[52] As a consequence, in a tight ion pair the counterion effect can be strong enough to make the S_1 and S_2 single excited states become degenerates and cross multiple times along the reaction pathway.

Figure 6 shows the MEP computed for the *cis→trans* isomerisation about the central bond of model **3a** in absence (dotted lines) and presence (bold lines) of a tight ion pair formed with the chloride ion. Concomitant destabilization of the ionic state and stabilization of the covalent single excited state induce degeneracy of S_1 and S_2 states, which stands for a significant part of the S_1 decay pathway. In the flat region of the S_1 energy profile, in fact, the counterion affects the electronic nature of the ionic state, which acquires a covalent character until the torsion restores a gap between the S_1 and S_2 surfaces and drives the system to a twisted minimum. This scenario may suggest that the *three-state* model could represent the photoisomerization process of a tight ion pair in vacuo more closely than the *two-state* model. However, it is worth to note that the ionic character is recovered on the reaction path before the one-bond flip is completed and the photoproduct is formed.
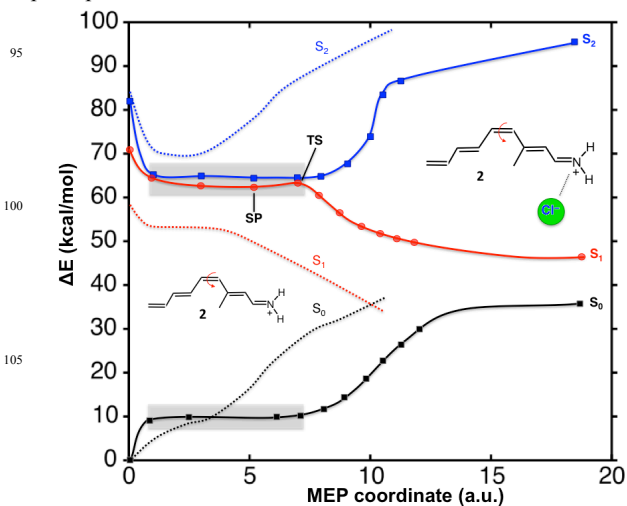
Figure 6. Computed MEPs along the S_1 photoisomerization coordinate of model **2** in presence of a chloride counterion in a tight ion pair (full lines) and in vacuo (dotted lines). Portion of energy surfaces characterized by covalent-like characters are highlighted with gray background. Reproduced from Ref. [53]

Notably, the position of the counterion can also affect the stereoselectivity of the isomerization reaction.[52] In particular,

moving the counterion above the molecular plane of the retinal chromophores allows for opening or locking specific isomerization paths,[78] with efficient barrierless photoisomerization pathways observed only for the double bond being closer to the negative charge. The observation that the position of the PSB counterion has the intrinsic potential to determine the type of retinal photochemistry (from ionic to covalent), to modulate its efficiency and to control the reaction selectivity has important implications on the fundamental understanding of PSB photoisomerization and provides essential information for the design of efficient PSB-based artificial photoswitchable devices.

The counterion quenching and the *opsin shift*

The computed MEP of the PSB/Cl⁻ ion pair in vacuo (Figure 6) indicates that the photoisomerization in tight PSB/anion pairs is significantly slower than in isolated PSBs. While this conclusion would be consistent with the slow PSB isomerization in solution (where tight ion pairs are indeed expected), it does not explain the ultrafast and efficient photoisomerization observed in retinal proteins (where a tight ion pair between the PSB chromophore and the carboxylate counterion is also observed). This inconsistency is due to the fact that the effective influence of the counterion on the chromophore photochemistry depends in turn on the PSB/anion surroundings. The hybrid QM/MM approach has been used to evaluate the role of protein cavity and solvent molecules on the spectral properties and the photochemistry of the PSB/anion tight ion pairs.[54, 55] A QM/MM study based on the crystal structure of bovine Rh at 2.8 Å resolution[79] provided computational evidences for the hypotheses formulated in the gas-phase studies of retinal chromophores.[21, 55, 68] In particular, the electronic character of S_1 and S_2 single excited states of the distorted PSB11 (according to its geometry in the protein) has been shown to be inverted from ionic to covalent for S_1, and vice versa for S_2, when moving from isolated PSB to the (isolated) tight ion pair PSB11(+)/E113(-). However, very notably, the ionic character of S_1 and the covalent nature of S_2 are preserved when the PSB11 is embedded in the electrostatic field of the protein matrix (including the E113 counterion), indicating that the protein cavity quenches the counterion effect (*counterion quenching*). The extent of this quenching effect has been debated in literature,[80-82] with two scenarios involving negligible protein effect (i.e. Rh absorbs as the isolate ion pair system)[80-82] to full shielding (i.e. Rh absorbs as the distorted PSB in vacuo). Accurate computations of the $S_0 \rightarrow S_1$ vertical excitations in bovine Rh and rigorous evaluation of the counterion quenching effect have been achieved[54] by employing a QM/MM method accounting for electrostatic embedding at the QM level,[35] and using the high-resolution (2.2 Å) X-ray data of bovine Rh.[83] Figure 7 shows the counterion (E113) effect on the computed $S_0 \rightarrow S_1$ vertical excitation of the PSB11 in its distorted geometric configuration, named PSB11$_{dist}$. The quenching effect of the protein cavity induces a red-shift which counterbalance 50% of the counterion blue-shift in bovine Rh, with major shielding contribution coming from the amino acid residues within 3.5 Å from the chromophore (Figure 7b). Such substantial counterion quenching is not observed for the PSB11/Cl⁻ ion pair in methanol solution,[35, 55] where both the tight and the loose ionic pairs show absorption maxima in the blue (453 and 442 nm, respectively),

very close to the absorption of isolated tight ion pairs. These QM/MM results indicate that in case of an unbound (i.e., loose) ionic pair the firsts solvation shells around the chromophore rearrange in a way that restores the counterion effect observed in bound (i.e., tight) ion pairs. Notably, the different spectral properties and counterion quenching extents observed for PSBs in solution versus protein (and vacuo) are in line with the different photochemistry experimentally observed: namely, counterion quenching seems to be a key ingredient for restoring an efficient and ultrafast photoisomerization of the retinal PSB chromophore (see also next section).
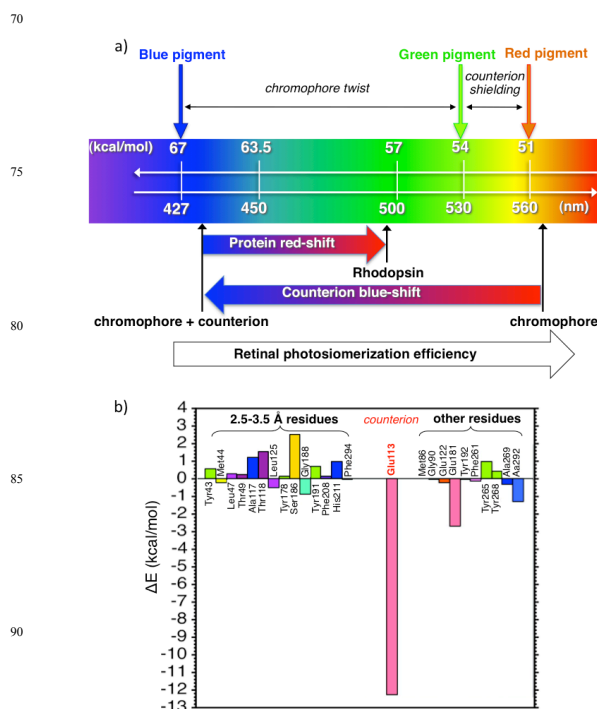

Figure 7. Spectral tuning and electrostatic effects in visual pigments. Panel a: spectral tuning in cone (blue, green and red) visual pigments and counterion and protein (shielding) electrostatic effects in Rh. Panel b: reverse fingerprint analysis of 14 rhodopsin residues comprised within a 2.5-3.5 Å radius around the chromophore, the counterion (Glu113), and other residues recognized relevant for spectral tuning in the visual pigments. Reproduced from Ref. [54]

The differences between electrostatic effects in solution and in the Rh protein suggest that the opsin protein environments have been evolutionary designed to tune the spectroscopic properties of the retinal chromophores (*opsin shift*). In fact, cones contain visual pigments that are maximally sensitive to long (L, red light), medium (M, green light) or short wavelengths (S, blue light) depending on the structure of the specific opsin protein (Figure 7a). It is hard to envision that the blue absorption in the short wavelengths pigments is entirely due to a lack of counterion quenching effect, since in such scenario the photoisomerization is expected to be very inefficient as shown in tight ion pairs. In fact, several factors must contribute to spectral tuning in vision, including twisting of the polyene chain of the chromophore due to steric strain, flexibility of the β-ionone ring, electrostatic effects in the protein binding pocket and specific PSB-counterion interactions (e.g., ion pair distance and H-bonding network). Very

recently, point mutagenesis experiments designed to alter electrostatics within the binding pocket of cellular retinol binding protein II, enabled full regulation of the absorption maximum of the retinal pigment in the range of 425 to 644 nm, indicating a strong influence of single amino acid residues on photophysical properties of PSBs.[84]

Eventually, the spectroscopic properties of several retinal molecules in vacuo have been experimentally and theoretically determined and suggested to be used as a new reference for the characterization of the "opsin effect" (i.e. the *opsin shift* with respect to the gas-phase).[23] Unfortunately, the crystal structures of cone visual pigments have not been resolved yet and the only available X-ray data that can be used to determine the various contributions to the visual spectral tuning are referred to Rh. In the next section we focus on the photochemistry of Rh, the visual pigment of rod cells and the reference proteic system for the study of primary events in vision.

Photoisomerization in rhodopsin

Among type II opsins, rhodopsin is the only GPCR for which the X-ray structures of the dark-adapted and the (all-*trans*) photointermediates have been resolved,[1-7] representing the reference system for fundamental studies of the vertebrate vision. The light-induced *cis→trans* isomerisation of the PSB11 in Rh (the so called *primary event* of vision) induces a series of conformational changes leading to the binding of the G-protein transducin, initiating the signal transduction processes in the visual cascade which ends with excitation of the visual nerve.[8] This primary reaction is an ultrafast, highly efficient and selective photochemical process. In the previous sections we have shown how the photophysical properties and photochemical behavior of retinal models in vacuo are similar to that of PSB11 in Rh. However, structural properties of the bound retinal and electrostatic effects in the protein binding pocket must play an important role in the *cis→trans* isomerisation of the PSB11 in Rh. For instance, *ab initio* molecular dynamics of the five-double-bond model of the PSB11 chromophore in vacuo (i.e. model **2** in the distorted configuration found in Rh) have shown how the geometric distortions induced by steric interaction with the protein pocket make the photoreaction very fast, stereoselective and highly efficient.[85]

Figure 8 shows the MEP calculated for PSB11 in Rh at the QM(CASSCF)/MM(AMBER) level,[54] based on the X-ray structural model of bovine Rh at 2.2 Å resolution.[83] The photoisomerization reaction coordinate has the same topology as documented previously for the retinal models in vacuo, i.e. a *two-mode* path involving first skeletal deformation and subsequent torsional motion. In the protein environment, however, the twisting motion is not a simple one-bond-flip mode along the central $C_{11}=C_{12}$ bond but a synergic torsional movement of adjacent C-C bonds in the chromophore central moiety, with a clockwise rotation of the C10—C11—C12—C13 dihedral angle coupled to a small counterclockwise change in the adjacent C8—C9—C10—C11 dihedral.[54, 55, 86] Such asynchronous motion resembles the Warshel's bicycle model,[65] with only little displacement of the retinal backbone ends ("space-saving" mechanism) and minimization of the steric interactions with the protein cavity. The direction of the twisting motion is also

reproduced by the QM/MM model, in agreement with simulations of chiroptical data.[36]

In the previous section, we have described the electrostatic effects of counterions on the photophysical and photochemical properties of PSB chromophores. The X-ray data of bovine Rh at 2.2 Å resolution[83] indicate the presence of two protonable amino acid side chains with carboxylate groups nearby the bound PSB11 chromophore, i.e. the amino acid residue Glu181 (E181) on the extracellular *loop 2* (E2) and the counterion E113. The protonation state of E181 in the dark-adapted state of Rh it has been matter of discussion in the literature.[87-93] However, the sidechain of E181 is located in proximity of the central twisting double bond, and it is expected not to affect the relative stabilities of the S_1 and S_2 single excited states and the photoisomerization path of the retinal chromophore (see Figure 5). In fact, the calculated MEPs shown in Figure 8a indicate that the isomerization path of PSB11 in Rh is not significantly affected by the protonation state of E181 (Figure 8a,b). Figure 8c highlights the importance of the counterion quenching effect, due to the protein environment, in triggering an efficient photoisomerization. This has been determined by computing the MEP in a protein environment where all external charges have been switched off except for the counterion charge (bold lines in Fig. 8c). Limiting the protein electrostatic effects to the E113 counterion charge alone reproduces the scenario of a fully unquenched counterion (as found in a tight ion pair in vacuo).
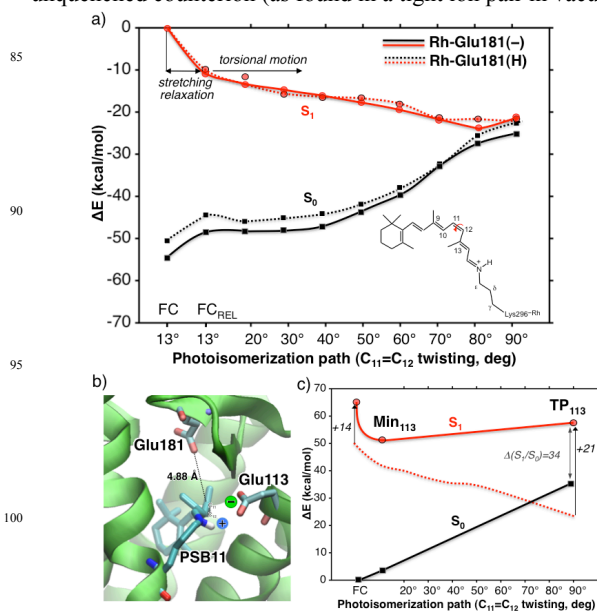

Figure 8. PSB11 photoisomerization in Rh. Panel a: CASPT2 corrected S_0 and S_1 energy profiles along the QM(CASSCF)/MM relaxed scan on S_1. tracing the photoisomerization process from the FC point to the twisted CI funnel, through a point (FC_{rel}) where only skeletal bond stretchings have been relaxed. Two different Rh setups with charged (full lines) and protonated (dotted lines) Glu181 side chain are reported. Panel b: retinal binding pocket in Rh according to X-ray data, with Glu181 placed right above the central double bond PSB11 and the Glu113 counterion in a tight ion pair. Panel c: energy profiles along the S_1 photoisomerization MEP computed in Rh (S_1, red dotted line) have been reevaluated in the protein accounting only for the counterion charge (full lines). Reproduced from Ref. [54]

As discussed in the previous section, a blue-shift is expected for the $S_0 \rightarrow S_1$ vertical excitation in the presence of a fully

unquenched counterion, which is estimated to be ~14 kcal/mol at the FC. Moving along the S_1 state path the charge transfer character of the state is increasing upon rotation, reaching a maximum at the CI point (~90° twisting angle) where a net charge transfer occurs and the highest blue-shift is expected. Here, in fact, a blue-shift of ~34 kcal/mol is estimated and the S_1/S_0 intersection funnel disappears, giving rise to a twisted point (TP$_{113}$) with a large S_1/S_0 energy gap separation (~21 kcal/mol; see Figure 8c). Therefore, removal of the protein electrostatic counterion quenching affects the slope of the S_1 photoisomerization path, with formation of an excited-state intermediate (Min$_{113}$) and appearance of a barrier at the twisted point. The protein environment in visual pigments is thus required to have an efficient and ultrafast photoisomerization since, by quenching the counterion (E113) effect, it guarantees a steep and barrierless isomerization path and a twisted CI funnel, as found in vacuo. Thus, modulation of the protein counterion shielding power allows for spectral tuning and regulation of the photoisomerization catalysis.

Time resolved (one-dimensional, 1D) pump-probe and stimulated fluorescence spectroscopies[41, 42] along with femtosecond-stimulated Raman spectroscpy[94] (FSRS) have been used to shed light on the molecular mechanism driving the unusually fast, efficient and selective *cis→trans* isomerisation reaction of PSB11 in Rh. Experimental evidences showed general agreement with the TSTM model proposed for retinal models in vacuo and in protein, with FSRS experiments suggesting for the first time the involvement of fast out-of-plane vibrations of the hydrogen atoms vicinal to the reacting double bond (HOOP mode) in driving the fast formation of the all-*trans* photoproduct. Ultrafast optical spectroscopy experiments with sub-20-fs time resolution in combination with scaled-CASSCF/AMBER molecular dynamics simulations have been recently reported,[37] providing compelling evidences of the existence of CI in Rh photochemistry, which is reached within 80 fs after photoexcitation (Figure 9a-c). Figure 9 shows the comparison between experimental (1D pump-probe) and simulated differential transmission ($\Delta T/T$) maps, determined as a function of pump–probe time delay and probe wavelength. At early probe delays, the photobleaching (blue) signal rising from the Rh ground state, peaking at ~510 nm, and the photoinduced excited-state absorption (namely a $S_1{\rightarrow}S_n$ transition, in red), peaking at ~500 nm, overlap in the visible region of the transient 1D spectrum (Fig. 9a, bottom panel). Within the first ~75 fs the stimulated emission (SE) signal rises from the wave packet initially created at FC region and evolves following the S_1 reaction pathway (positive blue signal in Fig. 9a, top panels), with a progressive shift of the SE signal to the red in the near-IR (NIR) region, up to wavelengths close to 1000 nm as the wave packet approaches the CI funnel and S_1-S_0 energy gap becomes smaller and smaller. The intensity decay of the SE signal is followed by the appearance of a symmetric weak photoinduced negative signal (red signal in Fig. 9a, top panels) at NIR wavelengths (~1000 nm) and at probe delays >80 fs. As depicted in figure 9c, the evident $\Delta T/T$ signal change at ~80 fs is due to the presence of the CI funnel, with the wave packet transferring from the S_1 surface to the hot ground state of the photoproduct. At time delays >200 fs after photoexcitation, the photoinduced negative signal has significantly increased its

intensity and it is stabilized with a strong peak at 560 nm, with the wave packet now moving in the GS of the all-*trans* photoproduct. As shown in Figure 9a the simulated $\Delta T/T$ map agrees almost quantitatively with the experimental one. The analysis of the QM/MM molecular dynamics indicated that the chromophore ends (yellow region in Figure 9b) remain essentially motionless during the fast photoisomerization, while minimal atomic displacements of the central carbon chain are necessary for effective *cis→trans* isomerisation, in agreement with other proposed mechanisms.[65, 86, 94]
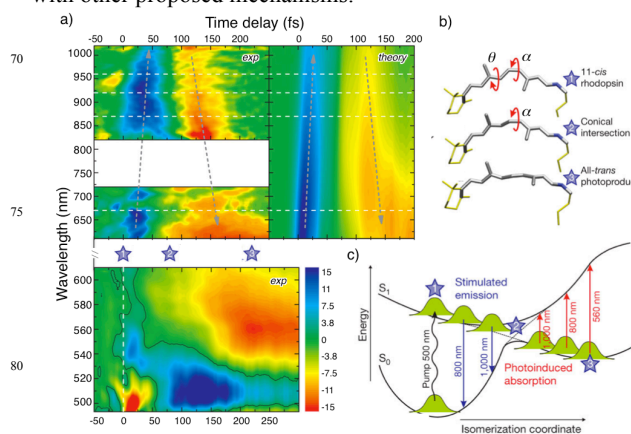

Figure 9. Wave-packet dynamics during photoisomerization in Rh. Panel a: Experimental and simulated differential transmission ($\Delta T/T$) maps as a function of time delay and wavelength in the visible (bottom panel) and NIR (top panels) spectral regions. Panels b,c: Averaged structures of the chromophore at the initial 11-*cis* (blue star '1', t=50 fs, α=-12.8°), CI (blue star '2', t=110 fs, α=-87.8°) and final all-*trans* (blue star '3', t=200 fs, , α=-141.0°) configurations (panel b) and the sketch of the ground- and excited-state potential energy surfaces (panel c). Arrows indicates photoexcitation (wavy), stimulated emission (blue) or photoinduced absorption (red/orange). Reproduced from Ref. [37]

Recently, the reason of the high efficiency of the all-*trans* product formation in Rh has been elucidated by analyzing an extended sample of hybrid QM(CASSCF)/MM trajectories at physiological conditions.[95] When the hopping to the ground state happens at the very first close encounter of the S_1/S_0 surfaces, a high probability (>80%) of yielding the trans photoproduct is observed, thus accounting for the high photoisomerization QY observed in Rh. Here, the C11=C12 carbon skeletal torsions proceeds essentially parallel to torsions of the C11 and C12 hydrogens, which is related to the HOOP mode.[96, 97] If the hop fails at the first encounter, it takes 3-4 S_1/S_0 approaches to observe a surface hopping event, after which rapid oscillations in the H–C=C–H torsion angle is detected in the majority of trajectories. For hops at a later stage, the probability of generating the all-*trans* product drops to ~50%, indicating a random photoisomerization process. Notably, the product formation is correlated to the phase (i.e., the direction) of the hydrogen torsions, since the fast hydrogen motions induce the pyramidalisation at the C11 and C12 carbon atoms, affecting the alignment of p-orbitals forming the π-bond of the photoproduct. These results suggest that the H–C=C–H torsions are strongly involved in determining the selectivity of the photoisomerization reaction in Rh, indicating that a specific excitation of HOOP motion, e.g. by a laser pulse, can be used to regulate the selectivity of the PSB11 photoisomerization.

Two-dimensional electronic spectroscopy

Time-resolved 1D pump-probe spectroscopy has been used to study the photoisomerization process in Rh by tracking coherent wave-packet motion from the FC region to the CI and finally to the photoproduct.[37] QM/MM molecular dynamics simulations reproduce quantitatively the spectroscopic data (Figure 9), suggesting a barrierless process and a steep energy surface of the spectroscopic S_1 state, following a *two-state* photoisomerization mechanism (Figure 4b). In the protein environment, the wave packet propagation along the S_1 profile is uncoupled to the covalent S_2 state surface, due to a large S_1/S_2 energy gap. However, the interplay between ionic and covalent states along the photoisomerization path can play a crucial role in solution.[98] In the previous sections, we have shown how a *three-state* model (Figure 4a) more closely represent the photoisomerization process of a tight ion pair in vacuo and such scenario could be also representative of the PSB11 photoisomerization in solution. Time-resolved 1D pump-probe experiments cannot provide clearly resolved signatures of electronic transitions involving the covalent S_2 state, since excitations from the spectroscopic S_1 state to S_2 fall in the infrared (IR), becoming strongly coupled with vibrational transitions and consequent loss of temporal resolution. Ideally, tracking $S_0 \rightarrow S_2$ transitions along the S_1 photoisomerization path could provide fundamental information on the relative positions of covalent and ionic states and eventually their electronic coupling. Elaborate multi-pulse techniques are required to probe such specific transitions and extract direct information on the role of covalent states in the PSB photoisomerization processes.
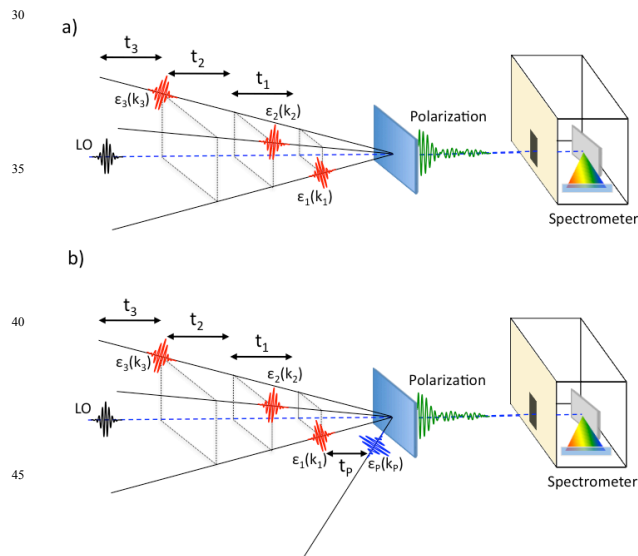

Figure 10. Schematic representation of heterodyne detected three-pulse photon echo (panel a) and transient 2D experimental setups (panel b); LO: local oscillator. Reproduced from Ref. [110]

Bidimensional (2D) spectroscopy has been established in the recent years as a powerful tool with high spectral resolution.[99-104] A sequence of two femtosecond pump pulses with variable time delay instead of a single pulse, as used in 1D pump-probe experiments, introduces an additional control parameter for manipulating the signal. As the information content of the nonlinear signal can be spread on two frequency axes, 2D spectroscopy provides a wealth of information on molecular structure and dynamics which remains hidden in 1D pump-probe experiments: pathway specific signals, molecular couplings, homogeneous and inhomogeneous broadening, etc.[100] The use of ultrashort pulses assures that the electric field emitted by the sample reflects the molecular response and allow for high time-resolution, as in 1D pump-probe experiments.

2D spectra in the IR (2DIR) and UV/Vis (2DUV/Vis) from third-order non-linear response of matter can be obtained by a heterodyne detected three-pulse photon echo experiment (Figure 10a).[105, 106] The emission of the four-wave-mixing signal has a background-free direction, which is heterodyned by a local oscillator (LO). Three ultrashort laser pulses interact in sequence with the sample, and the signal field emitted is detected as a function of the three controlled excitation-pulse time delays (t_1, t_2, and t_3). Double Fourier transformation with respect to time t_1 and t_3 generates the 2D spectrum (as a function of two frequencies, $\omega(t_1)$ "excitation frequency" and $\omega(t_3)$ "detection frequency") for a fixed value of the "waiting time" t_2 (or "population time"). By varying the (excited state) population time t_2, it is possible to monitor the relaxation of the excited states, in analogy to the pump–probe 1D experiments. With such three-pulse photon echo experiment setup the photoisomerization of retinals in protein and in solution can be monitored, with peaks broadening holding information on the frequency fluctuations and the spectral diffusion in different chromophore environments. Therefore, the time-resolved 2D spectroscopy (i.e., for $t_2>0$) could provide essential information on the dynamics of the first solvation shells (or amino acid residues) around the retinal chromophore that are hidden in 1D experiments.[107] However, the $S_0 \rightarrow S_2$ transitions during the photoisomerization on the S_1 surface are not directly probed by this technique. In fact, assuming a single spectroscopic state (S_1) and starting from the sample in equilibrium (in the GS, S_0 state), the first two laser pulses, ε_1 and ε_2 (with wave vectors k_1 and k_2, see Figure 10), allow for population and wave packet evolution along the S_1 states (for $t_2>0$). The third pulse, thus, can probe the $S_1 \rightarrow S_Y$ (where Y=0 or Y≥2) transitions during the wave packet evolution on the S_1 surface, respectively, and the $S_0 \rightarrow S_2$ transitions along the S_1 evolution are not probed.

Transient 2D (or "pump 2D-probe") spectroscopy is a subclass of fifth-order non-linear experiments that can be used to gain information on transient molecular states.[108, 109] Thereby, a femtosecond actinic UV/Vis pulse is used to disturb the sample and trigger the photochemical reaction. The UV spectrum of the generated transient state is measured in different time delays by means of 2D spectroscopy (vibrational or electronic), thus revealing information about the temporal evolution of the signal. In particular, transient 2DIR technique has been successfully applied to study unfolding and hydrogen bond dynamics of proteic systems.[108, 109] Here, we propose a transient 2DVis experiment for direct detection of $S_0 \rightarrow S_2$ transitions along the S_1 photoisomerization path of retinals. The transient experiment is conceived as follows (Figure 10b): an actinic pulse ε_P populates the reactive state S_1, thereby initiating the photoreaction. At variable time delays (t_P) the third-order nonlinear response of the system (in its transient state, i.e. along the S_1 reaction pathway) is generated using broadband femtosecond pulses in the Vis (i.e. ε_1,

ε_2 and ε_3 in Figure 10b). Therefore, as shown in Figure 11, different 2DVis spectra of the system evolving on the S_1 surface can be collected as function of the t_P delay.
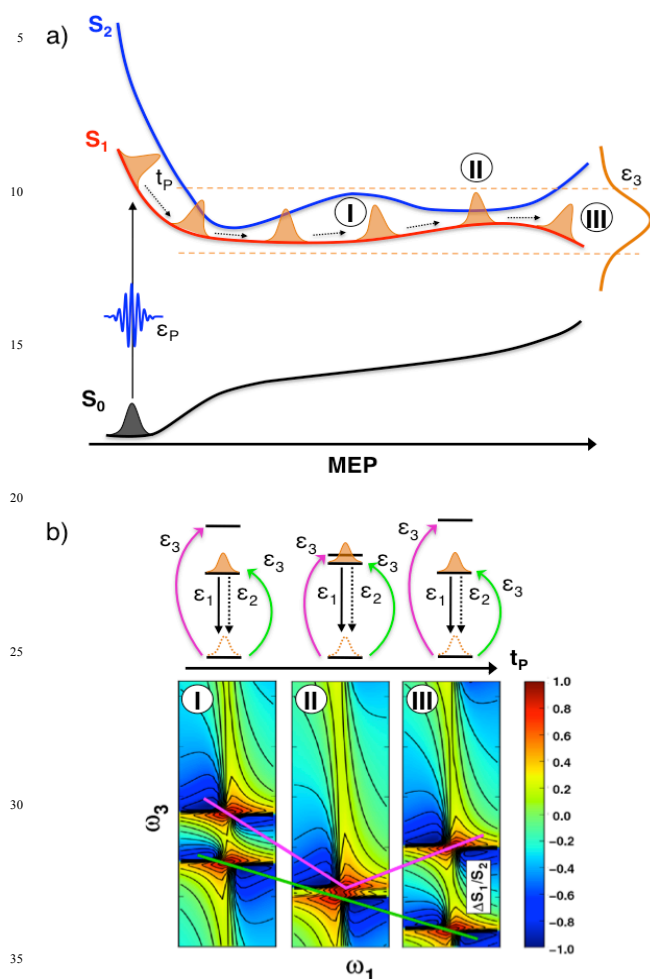

Figure 11. Schematic representation of the wave-packet evolution along the S_1 photoisomerization path of retinal chromophore (panel a) and idealized transient 2D spectra (panel b) collected at three different t_P delay times (I, II and III), showing the $S_0(t_P) \rightarrow S_2(t_P)$ transitions (off-diagonal red peaks, highlighted with magenta lines) and the $S_0(t_P) \rightarrow S_1(t_P)$ transitions (diagonal red peaks, highlighted with green line). These signals provide spectral signatures for the S_1/S_2 gap along the photoisomerization path.

Among the multiple feasible combinations of states that can be accessed (following the different Feynman pathways)[99] there is one where the two ε_1 and ε_2 pulses transfer population from the (evolving) S_1 state, $S_1(t_P)$, back to the ground state $S_0(t_P)$ (i.e., on the GS surface at time t_P) and the subsequent probe pulse ε_3 induces the $S_0(t_P) \rightarrow S_1(t_P)$ and $S_0(t_P) \rightarrow S_2(t_P)$ transitions. The $S_0(t_P) \rightarrow S_1(t_P)$ transition will manifest as a positive diagonal ($\omega_1 = \omega_3$) peak in the 2D spectra and it will red-shift as the S_0/S_1 gap decreases with increasing t_P delay (Figure 11b, red peaks and green line). If the S_2 state comes energetically close to the S_1 state along the reaction pathway (i.e., at different t_P delays) it will become resonant with the probe pulse and reveal itself in the 2D spectrum as a positive off-diagonal signal ($\omega_1 \neq \omega_3$). The appearance of the off-diagonal signal associated with the

$S_0(t_P) \rightarrow S_2(t_P)$ transition depends on the corresponding transition dipole moment, the position of the S_2 state relative to the S_1 state and the bandwidth of the probe pulse ε_3 (Figure 11b, red peaks and magenta lines). Notably, *ab initio* computations of the S_1 MEPs of retinal models in vacuo[68] and PSB11 in Rh[54, 55] as well as vertical excitations in solution[55] have shown that $S_0 \rightarrow S_2$ transitions have not negligible oscillator strengths at the FC and along the isomerization path. Thus, the time dependent S_1/S_2 splitting can be resolved spectroscopically exploiting the transient population of the ground state along the reaction pathway in a transient 2D experiment.

Due to the high density of excited states accessible by the proposed pulse sequence, the power of 2D spectroscopy to resolve different Feynman pathways becomes crucial. Essential for the application is to set the pump pulse ε_P in resonance with the frequency of the S_1 absorption in the FC region and the pulses ε_1, ε_2 and ε_3 in resonance with the red-shifted S_1 emission along the pathway. This will reduce the number of possible transitions (Feynman pathways) and will promote selection of the relevant peaks.

Design of tailored 2D experiments and analysis of transient 2D spectra is challenging and it demands precise knowledge of the singly and doubly excited manifolds of retinal along the relaxation pathway. Accurate simulations of 2DVis spectra can be achieved by employing our newly developed SOS//QM/MM protocol,[110] which combines molecular mechanics/quantum mechanics simulations with multiconfigurational wavefunction approaches and nonlinear spectroscopy techniques. Mixed quantum-classical dynamics simulations are needed to obtain a time-dependent picture and account for the inhomogeneous broadening that will be observed experimentally, as well as for quantum effects like population transfer between excited states. Synergisms between computational studies and transient 2D spectroscopy experiments represent a promising route to shed light on the photochemistry of retinals in protein environments and in solution, and photoactive biosystems in general.

Conclusions

In this Perspective, we review the last fifteen years of computational studies in our group that have been focused on the photophysical and photochemical properties of retinal models, and we introduce transient bidimensional (2D) optical spectroscopy as the ultimate conceivable experiment that could provide detailed information on the photoisomerization mechanism of retinals in different environments. The reviewed studies concern retinal models with increasing size, starting from the (three double bonds) minimal model of PSB in vacuo to the most recent QM/MM modeling of bound retinal in Rh. Multiconfigurational and multireference perturbative *ab initio* methods have been used to reveal the intrinsic photophysical and photochemical behavior of minimal retinal models. Computations of the MEP and *ab initio* on-the-fly semiclassical dynamics simulations in vacuo have suggested a photoisomerization mechanism involving a barrierless relaxation of the spectroscopic S_1 states from the FC region to a twisted conical intersection, providing a fast and efficient route to the photoproduct, in nice agreement with the short (sub-picosecond) time scale determined experimentally. Extensive computational analysis of the minimal,

methylated and long carbon-chain (up to unreduced) retinal models indicates a *two-state two-mode* mechanism for the photoisomerization process in vacuo, where *two-modes*, first skeletal deformations then torsions about the reacting double bond, characterize the molecular motion in the photoisomerization path and *two-states*, S_0 and S_1, are involved in the photoinduced wave packet dynamics. Environmental electrostatic effects, however, play a crucial role in determining the retinal photochemistry in protein and in solution. Due to the different (covalent or ionic) nature of the ground- and excited-states, the position of the PSB counterion determines the energy landscape of those states in vacuo (*counterion effect*), thus regulating the overall photoisomerization mechanism and modulating photochemical efficiency and reaction selectivity. For instance, *ab initio* computed MEPs for PSB/anion tight ion pairs in vacuo have suggested that a *three-state* model, involving the interplay between the ionic S_1 and the covalent S_2 states along the reaction path, represents the photoisomerization process more closely than a *two-state* model. The hybrid QM/MM approach has been used to evaluate environmental effects of protein cavity and solvent molecules on the spectral properties and the photochemistry of the PSB/anion tight ion pairs, indicating that the counterion effect observed in tight ion pairs in vacuo can be fully replaced by reorientation of polar solvent molecules around the PSB or can be quenched by the protein shielding (*counterion quenching*). Such remarkable electrostatic environmental effects suggest that protein cavities can be designed to finely tune the spectroscopic properties of retinal chromophores (*opsin shift*). Synergistic computational and experimental studies have provided the molecular movie of the photoisomerization process in bovine Rh with atomistic details and femtosecond resolution, providing fundamental insights on the PSB photochemistry in the proteic environment. The hybrid QM/MM model showed quantitative agreement with ultrafast optical spectroscopy (1D pump-probe) experiments, providing compelling evidences of the fast wave packet decay from the FC to the twisted CI, which is reached within 80 fs after photoexcitation. A space-saving mechanism with only little displacement of the retinal backbone ends and minimal steric interactions with the protein cavity characterizes the molecular motion during the 11-*cis*→all-*trans* isomerisation of the PSB, including fast HOOP vibrations that are strongly involved in determining the reaction selectivity. The observed very fast photoisomerization reaction in rhodopsin is consistent with a *two-state* mechanism, but experimental evidences of this mechanism cannot be achieved with time-resolved 1D or femtosecond-stimulated Raman spectroscopies. Here, we have proposed transient bidimensional (2D) optical spectroscopy with elaborate multi-pulse sequences as the ultimate experiment to shed light on the photoisomerization mechanisms in protein and in solution. In fact, the available computational studies and the experimental data indicate that a different interplay between the covalent (S_0 and S_2) states and the ionic (S_1) state could possible explain the fast and efficient photochemistry of bound retinals in protein (following a *two-state* mechanism) and the less efficient reactivity of solvated chromophores protein (following a *three-state* mechanism). In contrast to time-resolved 2D electronic spectroscopy, the proposed fifth-order non-linear experiments would allow for tracking both $S_0 \rightarrow S_1$ and $S_0 \rightarrow S_2$ transitions along the S_1 photoisomerization path and consequently the time dependent S_1/S_2 splitting can be resolved spectroscopically, providing direct information on the interplay between ionic and covalent excited states. To conclude, combination of transient 2D spectroscopy and accurate theoretical simulations of 2D electronic spectra could provide fundamental insights on retinals photochemistry in different environments and basic understanding for the design of efficient PSB-based artificial photoswitchable devices.

Notes and references

^a *Laboratoire de Chimie, Ecole Normale Supérieure de Lyon, 46, Allée d'Italie 69364 Lyon, France. FAX: +33-(0)-472728860; Tel:+33-(0)-472728811; E-mail:* ivan.rivalta@ens-lyon.fr*; E-mail:* marco.garavelli@ens-lyon.fr
^b *Dipartimento di Chimica "Giacomo Ciamician", Università di Bologna, via F. Selmi 2, 40126 Bologna, Italy. FAX: +39-(0)-512099456; Tel+39-(0)-512099545*

1. R. E. Stenkamp, S. Filipek, C. A. G. G. Driessen, D. C. Teller and K. Palczewski, *Bba-Biomembranes*, 2002, **1565**, 168-182.

2. D. Salom, D. T. Lodowski, R. E. Stenkamp, I. Le Trong, M. Golczak, B. Jastrzebska, T. Harris, J. A. Ballesteros and K. Palczewski, *Proc. Natl. Acad. Sci. USA*, 2006, **103**, 16123-16128.

3. K. Palczewski, T. Kumasaka, T. Hori, C. A. Behnke, H. Motoshima, B. A. Fox, I. Le Trong, D. C. Teller, T. Okada, R. E. Stenkamp, M. Yamamoto and M. Miyano, *Science*, 2000, **289**, 739-745.

4. J. Li, P. C. Edwards, M. Burghammer, C. Villa and G. F. X. Schertler, *J. Mol. Biol.*, 2004, **343**, 1409-1438.

5. H. Nakamichi and T. Okada, *Proc. Natl. Acad. Sci. USA*, 2006, **103**, 12729-12734.

6. H. Nakamichi and T. Okada, *Angewandte Chemie-International Edition*, 2006, **45**, 4270-4273.

7. H. W. Choe, Y. J. Kim, J. H. Park, T. Morizumi, E. F. Pai, N. Krauss, K. P. Hofmann, P. Scheerer and O. P. Ernst, *Nature*, 2011, **471**, 651-U137.

8. D. Baylor, *Proc. Natl. Acad. Sci. USA*, 1996, **93**, 560-565.

9. R. R. Birge, *Annu. Rev. Phys. Chem.*, 1990, **41**, 683-733.

10. J. Briand, O. Bram, J. Rehault, J. Leonard, A. Cannizzo, M. Chergui, V. Zanirato, M. Olivucci, J. Helbing and S. Haacke, *PCCP*, 2010, **12**, 3178-3187.

11. F. Lumento, V. Zanirato, S. Fusi, E. Busi, L. Latterini, F. Elisei, A. Sinicropi, T. Andruniow, N. Ferre, R. Basosi and M. Olivucci, *Angewandte Chemie-International Edition*, 2007, **46**, 414-420.

12. K. J. Wise, N. B. Gillespie, J. A. Stuart, M. P. Krebs and R. R. Birge, *Trends Biotechnol.*, 2002, **20**, 387-394.

13. I. B. Nielsen, M. A. Petersen, L. Lammich, M. B. Nielsen and L. H. Andersen, *J. Phys. Chem. A*, 2006, **110**, 12592-12596.

14. I. B. Nielsen, L. Lammich and L. H. Andersen, *Phys. Rev. Lett.*, 2006, **96**.

15. M. A. Petersen, I. B. Nielsen, M. B. Kristensen, A. Kadziola, L. Lammich, L. H. Andersen and M. B. Nielsen, *Organic & Biomolecular Chemistry*, 2006, **4**, 1546-1554.

16. L. H. Andersen, I. B. Nielsen, M. B. Kristensen, M. O. A. El Ghazaly, S. Haacke, M. B. Nielsen and M. A. Petersen, *J. Am. Chem. Soc.*, 2005, **127**, 12347-12350.

17. M. Garavelli, P. Celani, F. Bernardi, M. A. Robb and M. Olivucci, *J. Am. Chem. Soc.*, 1997, **119**, 6891-6901.

18. T. Vreven, F. Bernardi, M. Garavelli, M. Olivucci, M. A. Robb and H. B. Schlegel, *J. Am. Chem. Soc.*, 1997, **119**, 12687-12688.

19. M. Garavelli, T. Vreven, P. Celani, F. Bernardi, M. A. Robb and M. Olivucci, *J. Am. Chem. Soc.*, 1998, **120**, 1285-1288.

20. M. Garavelli, F. Negri and M. Olivucci, *J. Am. Chem. Soc.*, 1999, **121**, 1023-1029.

21. R. Gonzalez-Luque, M. Garavelli, F. Bernardi, M. Merchan, M. A. Robb and M. Olivucci, *Proc. Natl. Acad. Sci. USA*, 2000, **97**, 9379-9384.

22. A. Cembran, R. Gonzalez-Luque, P. Altoe, M. Merchan, F. Bernardi, M. Olivucci and M. Garavelli, *J. Phys. Chem. A*, 2005, **109**, 6597-6605.

23. J. Rajput, D. B. Rahbek, L. H. Andersen, A. Hirshfeld, M. Sheves, P. Altoe, G. Orlandi and M. Garavelli, *Angewandte Chemie-International Edition*, 2010, **49**, 1790-1793.

24. M. Barbatti, M. Ruckenbauer, J. J. Szymczak, A. J. A. Aquino and H. Lischka, *Physical Chemistry Chemical Physics*, 2008, **10**, 482-494.

25. M. Schreiber, M. Sugihara, T. Okada and V. Buss, *Angewandte Chemie-International Edition*, 2006, **45**, 4274-4277.

26. J. J. Szymczak, M. Barbatti and H. Lischka, *J. Phys. Chem. A*, 2009, **113**, 11907-11918.

27. O. Weingart, I. Schapiro and V. Buss, *Journal of Molecular Modeling*, 2006, **12**, 713-721.

28. O. Weingart, I. Schapiro and V. Buss, *Journal of Physical Chemistry B*, 2007, **111**, 3782-3788.

29. V. Buss, *Chirality*, 2001, **13**, 13-23.

30. O. Valsson and C. Filippi, *Journal of Chemical Theory and Computation*, 2010, **6**, 1275-1292.

31. E. Coccia, D. Varsano and L. Guidoni, *Journal of Chemical Theory and Computation*, 2013, **9**, 8-12.

32. D. Hegarty and M. A. Robb, *Mol. Phys.*, 1979, **38**, 1795-1812.

33. B. O. Roos, *Ab Initio Methods in Quantum Chemistry: part II*, Wiley, Chicester, U.K., 1987.

34. K. Andersson, P. A. Malmqvist and B. O. Roos, *J. Chem. Phys.*, 1992, **96**, 1218-1226.

35. P. Altoe, M. Stenta, A. Bottoni and M. Garavelli, *Theor. Chem. Acc.*, 2007, **118**, 219-240.

36. V. Buss, K. Kolster, F. Terstegen and R. Vahrenhorst, *Angewandte Chemie-International Edition*, 1998, **37**, 1893-1895.

37. D. Polli, P. Altoe, O. Weingart, K. M. Spillane, C. Manzoni, D. Brida, G. Tomasello, G. Orlandi, P. Kukura, R. A. Mathies, M. Garavelli and G. Cerullo, *Nature*, 2010, **467**, 440-U488.

38. S. Ruhman, B. X. Hou, N. Friedman, M. Ottolenghi and M. Sheves, *J. Am. Chem. Soc.*, 2002, **124**, 8854-8858.

39. T. Kobayashi, T. Saito and H. Ohtani, *Nature*, 2001, **414**, 531-534.

40. B. Hou, N. Friedman, S. Ruhman, M. Sheves and M. Ottolenghi, *J. Phys. Chem. B*, 2001, **105**, 7042-7048.

41. G. Haran, E. A. Morlino, J. Matthes, R. H. Callender and R. M. Hochstrasser, *J. Phys. Chem. A*, 1999, **103**, 2202-2207.

42. H. Kandori, Y. Furutani, S. Nishimura, Y. Shichida, H. Chosrowjan, Y. Shibata and N. Mataga, *Chem. Phys. Lett.*, 2001, **334**, 271-276.

43. S. L. Logunov, V. V. Volkov, M. Braun and M. A. El-Sayed, *Proc. Natl. Acad. Sci. USA*, 2001, **98**, 8475-8479.

44. H. Kandori, H. Sasabe, K. Nakanishi, T. Yoshizawa, T. Mizukami and Y. Shichida, *J. Am. Chem. Soc.*, 1996, **118**, 1002-1005.

45. H. J. Dartnall, *Vision Res.*, 1967, **7**, 1-&.

46. R. W. Schoenlein, L. A. Peteanu, R. A. Mathies and C. V. Shank, *Science*, 1991, **254**, 412-415.

47. R. A. Mathies, C. H. B. Cruz, W. T. Pollard and C. V. Shank, *Science*, 1988, **240**, 777-779.

48. H. Kandori, Y. Katsuta, M. Ito and H. Sasabe, *J. Am. Chem. Soc.*, 1995, **117**, 2669-2670.

49. S. L. Logunov, L. Song and M. A. ElSayed, *J. Phys. Chem.*, 1996, **100**, 18586-18591.

50. P. Hamm, M. Zurek, T. Roschinger, H. Patzelt, D. Oesterhelt and W. Zinth, *Chem. Phys. Lett.*, 1996, **263**, 613-621.

51. R. S. Becker and K. Freedman, *J. Am. Chem. Soc.*, 1985, **107**, 1477-1485.

52. A. Cembran, F. Bernardi, M. Olivucci and M. Garavelli, *J. Am. Chem. Soc.*, 2004, **126**, 16018-16037.

53. A. Cembran, F. Bernardi, M. Olivucci and M. Garavelli, *Proc. Natl. Acad. Sci. USA*, 2005, **102**, 6255-6260.

54. G. Tomasello, G. Olaso-Gonzalez, P. Altoe, M. Stenta, L. Serrano-Andres, M. Merchan, G. Orlandi, A. Bottoni and M. Garavelli, *J. Am. Chem. Soc.*, 2009, **131**, 5172-5186.

55. T. Andruniow, N. Ferre and M. Olivucci, *Proc. Natl. Acad. Sci. USA*, 2004, **101**, 17908-17913.

56. J. C. Tully and R. K. Preston, *J. Chem. Phys.*, 1971, **55**, 562-&.

57. B. R. Smith, M. J. Bearpark, M. A. Robb, F. Bernardi and M. Olivucci, *Chem. Phys. Lett.*, 1995, **242**, 27-32.

58. O. Weingart, A. Migani, M. Olivucci, M. A. Robb, V. Buss and P. Hunt, *J. Phys. Chem. A*, 2004, **108**, 4685-4693.

59. G. G. Kochendoerfer and R. A. Mathies, *J. Phys. Chem.*, 1996, **100**, 14526.

60. Q. Wang, R. W. Schoenlein, L. A. Peteanu, R. A. Mathies and C. V. Shank, *Science*, 1994, **266**, 422.

61. R. W. Schoenlein, L. A. Peteanu, R. A. Mathies and C. V. Shank, *Science*, 1991, **254**, 412.

62. G. Haran, K. Wynne, A. Xie, Q. He, M. Chance and R. M. Hochstrasser, *Chem. Phys. Lett.*, 1996, **261**, 389.

63. J. K. Delaney, T. L. Brack, G. H. Atkinson, M. Ottolenghi, G. Steinberg and M. Sheves, *Proc. Natl. Acad. Sci. USA*, 1995, **92**, 2101-2105.

64. A. Warshel and M. Karplus, *Chem. Phys. Lett.*, 1975, **32**, 11.

65. A. Warshel, *Nature*, 1976, **260**, 679-683.

66. A. Warshel, *Proc. Natl. Acad. Sci. USA*, 1978, **75**, 2558-2562.

67. A. Warshel, Z. T. Chu and J. K. Hwang, *Chem. Phys.*, 1991, **158**, 303-314.

68. A. Cembran, R. Gonzalez-Luque, L. Serrano-Andres, M. Merchan and M. Garavelli, *Theor. Chem. Acc.*, 2007, **118**, 173-183.

69. G. G. Kochendoerfer and R. A. Mathies, *J. Phys. Chem.*, 1996, **100**, 14526-14532.

70. H. Chosrowjan, N. Mataga, Y. Shibata, S. Tachibanaki, H. Kandori, Y. Shichida, T. Okada and T. Kouyama, *J. Am. Chem. Soc.*, 1998, **120**, 9706-9707.

71. F. Gai, K. C. Hasson, J. C. McDonald and P. A. Anfinrud, *Science*, 1998, **279**, 1886-1891.

72. K. Schulten, W. Humphrey, I. Logunov, M. Sheves and D. Xu, *Isr. J. Chem.*, 1995, **35**, 447-464.

73. R. M. Weiss and A. Warshel, *J. Am. Chem. Soc.*, 1979, **101**, 6131-6133.

74. J. B. Hurley, T. G. Ebrey, B. Honig and M. Ottolenghi, *Nature*, 1977, **270**, 540-542.

75. M. Ruckenbauer, M. Barbatti, T. Muller and H. Lischka, *J. Phys. Chem. A*, 2010, **114**, 6757-6765.

76. A. J. A. Aquino, M. Barbatti and H. Lischka, *Chemphyschem*, 2006, **7**, 2089-2096.

77. M. Ruckenbauer, M. Barbatti, T. Mueller and H. Lischka, *J. Phys. Chem. A*, 2013, **117**, 2790-2799.

78. T. J. Martinez, *Acc. Chem. Res.*, 2006, **39**, 119-126.

79. D. C. Teller, T. Okada, C. A. Behnke, K. Palczewski and R. E. Stenkamp, *Biochemistry*, 2001, **40**, 7761-7772.

80. A. Altun, S. Yokoyama and K. Morokuma, *J. Phys. Chem. B*, 2008, **112**, 6814-6827.

81. S. Sekharan, M. Sugihara and V. Buss, *Angewandte Chemie-International Edition*, 2007, **46**, 269-271.

82. K. Fujimoto, S. Hayashi, J. Hasegawa and H. Nakatsuji, *Journal of Chemical Theory and Computation*, 2007, **3**, 605-618.

83. T. Okada, M. Sugihara, A. N. Bondar, M. Elstner, P. Entel and V. Buss, *J. Mol. Biol.*, 2004, **342**, 571-583.

84. W. J. Wang, Z. Nossoni, T. Berbasova, C. T. Watson, I. Yapici, K. S. S. Lee, C. Vasileiou, J. H. Geiger and B. Borhan, *Science*, 2012, **338**, 1340-1343.

85. O. Weingart, *J. Am. Chem. Soc.*, 2007, **129**, 10618-+.

86. L. M. Frutos, T. Andruniow, F. Santoro, N. Ferre and M. Olivucci, *Proc. Natl. Acad. Sci. USA*, 2007, **104**, 7764-7769.

87. E. C. Y. Yan, M. A. Kazmi, Z. Ganim, J. M. Hou, D. H. Pan, B. S. W. Chang, T. P. Sakmar and R. A. Mathies, *Proc. Natl. Acad. Sci. USA*, 2003, **100**, 9262-9267.

88. E. C. Y. Yan, M. A. Kazmi, S. De, B. S. W. Chang, C. Seibert, E. P. Marin, R. A. Mathies and T. P. Sakmar, *Biochemistry*, 2002, **41**, 3620-3627.

89. R. R. Birge, L. P. Murray, B. M. Pierce, H. Akita, V. Baloghnair, L. A. Findsen and K. Nakanishi, *Proc. Natl. Acad. Sci. USA*, 1985, **82**, 4117-4121.

90. A. Terakita, T. Yamashita and Y. Shichida, *Proc. Natl. Acad. Sci. USA*, 2000, **97**, 14263-14267.

91. U. F. Rohrig, L. Guidoni and U. Rothlisberger, *Biophys. J.*, 2002, **82**, 223A-223A.

92. S. Ludeke, R. Beck, E. C. Y. Yan, T. P. Sakmar, F. Siebert and R. Vogel, *J. Mol. Biol.*, 2005, **353**, 345-356.

93. J. W. Lewis, I. Szundi, M. A. Kazmi, T. P. Sakmar and D. S. Kliger, *Biochemistry*, 2004, **43**, 12614-12621.

94. P. Kukura, D. W. McCamant, S. Yoon, D. B. Wandschneider and R. A. Mathies, *Science*, 2005, **310**, 1006-1009.

95. O. Weingart, P. Altoe, M. Stenta, A. Bottoni, G. Orlandi and M. Garavelli, *PCCP*, 2011, **13**, 3645-3648.

96. O. Weingart, *Chem. Phys.*, 2008, **349**, 348-355.

97. N. Klaffki, O. Weingart, M. Garavelli and E. Spohr, *PCCP*, 2012, **14**, 14299-14305.

98. G. Zgrablic, K. Voitchovsky, M. Kindermann, S. Haacke and M. Chergui, *Biophys. J.*, 2005, **88**, 2779-2788.

99. S. Mukamel, *Principles of nonlinear optical spectroscopy*, New York, O.U.P., 1995.

100. P. Hamm and M. Zanni, *Concepts and Methods of 2D Infrared Spectroscopy*, Cambridge University Press, 2011.

101. W. Zhuang, T. Hayashi and S. Mukamel, *Angewandte Chemie-International Edition*, 2009, **48**, 3750-3781.

102. M. T. Zanni and R. M. Hochstrasser, *Curr. Opin. Struct. Biol.*, 2001, **11**, 516-522.

103. S. Mukamel, *Annu. Rev. Phys. Chem.*, 2000, **51**, 691-729.

104. B. A. West and A. M. Moran, *Journal of Physical Chemistry Letters*, 2012, **3**, 2575-2581.

105. T. Brixner, I. V. Stiopkin and G. R. Fleming, *Opt. Lett.*, 2004, **29**, 884-886.

106. M. L. Cowan, J. P. Ogilvie and R. J. D. Miller, *Chem. Phys. Lett.*, 2004, **386**, 184-189.

107. S. T. Roberts, J. J. Loparo and A. Tokmakoff, *J. Chem. Phys.*, 2006, **125**.

108. C. Kolano, J. Helbing, M. Kozinski, W. Sander and P. Hamm, *Nature*, 2006, **444**, 469-472.

109. H. S. Chung, Z. Ganim, K. C. Jones and A. Tokmakoff, *Proc. Natl. Acad. Sci. USA*, 2007, **104**, 14237-14242.

110. I. Rivalta, A. Nenov, G. Cerullo, S. Mukamel and M. Garavelli, *Int. J. Quantum Chem*, 2014, **114**, 85-93.